Preparation of Ce-doped 001-TiO_2 Photocatalyst and Study on Its High-Efficiency Photocatalytic Degradation Performance and Mechanism for perfluorooctanoic acid

Wenqin Zeng[1,*], Chen Xie[2], Jintao Wang[3,*], Tongshuai Rong[4], Feng Zhou[2], Bohao Zhao[2]
[1]Vocational Technical College, Yongzhou, 425000, China
[2]Rocket Force University of Engineering, Xi'an 710025, China
[3]Shaanxi Province High-Tech Institute of Xi'an, No. 2, Tongxin Road, Baqiao District, Xi 'an City, China
[4]Yantai Laiyang Environmental Monitoring Center
*Corresponding author: Wenqin Zeng, hnyzzhen@163.com and Jintao Wang, wangjintaolove@126.com

Abstract: Perfluorooctanoic acid (PFOA) is widely used in industrial and commercial applications. Prolonged exposure to perfluorooctanoic acid can lead to developmental and reproductive toxicity, liver damage, endocrine disruption, and potential carcinogenicity, posing a severe threat to both the ecological environment and human health. Therefore, there is an urgent need to develop an efficient and environmentally friendly technology for perfluorooctanoic acid wastewater treatment. Photocatalytic technology has attracted significant attention due to its low cost and environmental friendliness, with the key focus being the development of highly efficient photocatalysts. In this study, Ce-doped 001-TiO_2 was prepared using a solvothermal method. Its microstructure, morphology, and photoelectric properties were characterized by various methods. The degradation performance of this catalyst towards simulated perfluorooctanoic acid wastewater under visible light was also investigated. The results demonstrated that Ce/001-TiO_2 exhibited good dispersion. The synergistic effect of crystal facet modulation and Ce doping facilitated efficient spatial separation and transfer of photogenerated carriers, resulting in a reduced bandgap and an expanded light absorption range for the composite photocatalyst, thereby significantly enhancing its photocatalytic performance. Under simulated sunlight irradiation, Ce/001-TiO_2 achieved a 95.4% degradation efficiency for high-concentration perfluorooctanoic acid perfluorooctanoic acid wastewater (5 mg/L) within 240 minutes. This study provides a feasible and practical approach for the efficient degradation of perfluorooctanoic acid wastewater.

Keywords: Photocatalysis, Perfluorooctanoic Acid, Ce-Doped 001-TiO_2，Degradation

1 Introduction

Perfluorinated compounds (PFCs), as a class of synthetic and persistent organic compounds, exhibit unique surface-active properties and exceptional chemical stability. Since the mid-20th century, PFCs have been widely applied in industrial and commercial sectors [1-2]. With the surge in PFC production and the expansion of their usage scope, these substances have been frequently detected in various environmental media worldwide, with perfluorooctanoic acid (PFOA) being the most prevalent [3]. The high electronegativity of fluorine atoms (F) and the extremely high bond energy of carbon-fluorine bonds (C—F) in PFOA molecules render PFOA resistant to degradation and biotransformation processes [4-5]. PFOA is associated with a range of adverse health effects from long-term exposure, including developmental and reproductive toxicity, hepatotoxicity, endocrine disruption, and potential carcinogenicity [6]. Therefore, the development of cost-effective, efficient, and environmentally friendly PFOA removal technologies has emerged as a critical challenge in the field of environmental science [7].

Conventional approaches such as physical adsorption and biological treatment face fundamental limitations in achieving efficient PFOA elimination. In some cases, these processes may even lead to elevated PFOA levels through mechanisms like media saturation and biological accumulation [8]. In contrast, photocatalytic technology demonstrates significant advantages in PFOA wastewater treatment owing to its environmental friendliness, operational safety, and sustainable purification characteristics. Among numerous photocatalytic materials, TiO_2 stands out due to its non-toxicity, low cost, and tunable morphology, offering broad application prospects in environmental pollution control [9-11]. For instance, Dillert et al. pioneered the study of PFOA degradation via UV-light-driven photocatalysis using TiO_2 as a catalyst under acidic conditions, although the initial degradation efficiency required improvement. Research on the degradation mechanism revealed that TiO_2 generates photogenerated electrons and holes under light excitation, where electrons react with oxygen to form superoxide radicals, while holes, with their strong oxidizing capacity, react with water to produce hydroxyl radicals. These two reactive species synergistically

mineralize PFOA [12]. Studies have shown that the surface energies of low-index crystal facets of anatase TiO_2 follow the order of (001) (0.90 J/m²) > (100) (0.53 J/m²) > (101) (0.44 J/m²), with the high-energy (001) facet significantly enhancing photocatalytic reactivity due to its abundance of five-coordinate titanium atoms (Ti5c) and a larger Ti-O-Ti bond angle [13]. Current research confirms that selective exposure of the {001} facet enables directional enrichment of photogenerated holes, thereby accelerating the kinetics of photocatalytic oxidation reactions. This facet-engineering strategy establishes a solid foundation for the rational design of high-performance TiO_2-based photocatalytic materials [14].

However, the photocatalytic performance of single-phase TiO_2 is constrained by its narrow spectral response range and weak internal driving force for photogenerated carrier separation, limiting its photocatalytic activity to suboptimal levels. Therefore, doping modification strategies are necessary to tailor the crystal structure and optical properties of TiO_2 to enhance catalyst activity [15]. Cerium (Ce), with its unique 4f electron configuration and abundant surface oxygen defects, features a Ce^{4+}/Ce^{3+} redox couple that serves as an efficient charge transfer mediator, precisely regulating the generation of reactive species [16]. When Ce is successfully doped into TiO_2 with exposed (001) facets, the synergistic effects of facet engineering and Ce doping enable efficient modulation of charge generation and transfer processes at the photocatalyst's surface-interface, substantially improving carrier separation efficiency and yielding photocatalytic materials with both high activity and stability [17].

Given the widespread presence and recalcitrant nature of PFCs in various wastewaters and sewage, this study synthesized Ce/001-TiO_2 via a solvothermal method and comprehensively investigated its physicochemical and photoelectric properties using multiple characterization techniques. Under simulated solar irradiation, efficient removal of PFOA was achieved, and a plausible photocatalytic degradation mechanism for PFOA was proposed. The findings of this research offer scientific insights and technical support for the development of cost-effective, rational, and feasible PFOA wastewater treatment technologies.

2 Experimental Section

2.1 Materials

Tetrabutyl titanate (TBT) and titanium tetrafluoride were procured from Aladdin (Shanghai, China). Standard perfluorocarboxylic acids (PFCAs, C_2–C_8) with carbon chain lengths ranging from 2 to 8 were obtained from ANPEL (Shanghai, China). Hydrochloric acid (HCl, AR grade), nitric acid (HNO_3, AR grade), and sodium hydroxide (NaOH, AR grade) were supplied by Sanpu Chemical Reagent Co., Ltd. (Xi'an, China). Anhydrous ethanol (AR grade) was purchased from Hengxing Chemical Reagent Co., Ltd. (Tianjin, China). Cerium nitrate hexahydrate (AR grade, >99.99%) was sourced from Aladdin Chemical Reagents Co., Ltd. Isopropanol, p-benzoquinone, ethylenediaminetetraacetic acid disodium salt (EDTA-2Na), and carbon tetrachloride (all >99.99%, AR grade) were also obtained from Aladdin Chemical Reagents Co., Ltd. Deionized water was prepared in-house in the laboratory. All reagents were of analytical grade and used without further purification.

2.2 Fabrication of photocatalysts

Fabrication of Ce/001-TiO_2 : The 001-TiO_2 was synthesized via a hydrothermal method. Under high-speed stirring using a magnetic stirring apparatus, 2.5 mL of titanium tetrafluoride and 12.5 mL of tetrabutyl titanate (TBT) were sequentially added dropwise to a tert-butanol solution to form a homogeneous mixture. Subsequently, 0.2 g of cerium nitrate hexahydrate was introduced, and the suspension was continuously stirred for 1 h. The resulting suspension was then transferred to a stainless-steel autoclave lined with polytetrafluoroethylene (PTFE) and subjected to a hydrothermal reaction at 200 °C for 6 h. After the autoclave naturally cooled to room temperature, the solid product was collected by vacuum filtration and alternately washed multiple times with deionized water and anhydrous ethanol. The white solid was then separated by centrifugation at 6000 rpm for 50 min using a high-speed centrifuge. Following additional alternating washes with deionized water and anhydrous ethanol, the product was dried in an oven at 80 °C and carefully ground. The resulting white powder, denoted as Ce/001-TiO_2, consisted of cerium-doped titanium dioxide nanosheets with a high exposure of (001) crystal facets.

2.3 Material Characterization

The phase composition and crystallographic structure of the as-synthesized samples were characterized by X-ray diffraction (XRD, Bruker D8 Advanced, Germany) using Cu Kα radiation (λ = 0.15401 nm) operated at 40 kV. Data were collected over a 2θ range of 5°–90° at a scanning rate of 5°/min.

X-ray photoelectron spectroscopy (XPS, AXIS ULTRADLD, UK) was employed to analyze the surface elemental composition and chemical states, with all binding energies referenced to the C 1s peak at 284.8 eV. Morphological features and surface elemental distribution were examined by field-emission scanning electron microscopy (FESEM, Gemini, Germany) coupled with energy-dispersive X-ray spectroscopy (EDS) at an acceleration voltage of 15 kV. Further microstructural and crystallographic information was obtained using high-resolution transmission electron microscopy (HRTEM, JEM-2100F, JEOL, Japan), from which interplanar spacings were derived.

Optical absorption properties were evaluated by ultraviolet–visible diffuse reflectance spectroscopy (UV–Vis DRS) on a UV–Vis spectrometer (Ocean Optics SB650, USA). Steady-state photoluminescence (PL) spectra were acquired using a fluorescence spectrometer (F-7000, Hitachi, Japan) with an excitation wavelength of 325 nm. Electron paramagnetic resonance (EPR, Bruker A300, Germany) was utilized to detect and identify radical species. Photoelectrochemical performance was assessed via chronoamperometry using an electrochemical workstation (Princeton P4000, USA). The concentration of perfluorooctanoic acid (PFOA) was quantified by high-performance liquid chromatography (HPLC, Ultimate 3000, USA).

2.4 Methods of Analysis

The photocatalytic performance of the prepared samples was evaluated by monitoring the degradation efficiency of simulated perfluorooctanoic acid (PFOA) wastewater under xenon lamp irradiation. A CEL-LAB500E 350 W xenon lamp equipped with an AM 1.5 filter was employed to simulate solar light, with the light intensity set at 100 mW/cm². The catalyst was dispersed in 50 mL of PFOA wastewater (5 mg/L) and magnetically stirred in the dark for 30 min to establish adsorption-desorption equilibrium. Subsequently, the xenon lamp was turned on to initiate the photocatalytic reaction. After the reaction, the suspension was centrifuged, and the absorbance (A) of the supernatant was measured.

The photocatalytic performance was assessed using the degradation efficiency (R) of PFOA wastewater and reaction kinetics, as described by the following equation:

$$R = \frac{C_0 - C_t}{C_0} \times 100\% \quad (1)$$

Where C_0 is the initial concentration of PFOA wastewater (mg/L), and C_t is the concentration of PFOA wastewater at time t (mg/L) during photocatalytic degradation.High-performance liquid chromatography (HPLC) was employed for the quantitative determination of PFOA in the wastewater.

Generally, the photocatalytic degradation of organic pollutants in aqueous systems follows pseudo-first-order kinetics, and the rate constant (k) provides a direct measure of the degradation rate, as expressed by:

$$\ln\left(\frac{C_0}{C_t}\right) = k \times t \quad (2)$$

3 Results and Discussions

The transmission electron microscopy (TEM) characterization results reveal the morphological features of both 001-TiO_2 and Ce/001-TiO_2. The TEM image of 001-TiO_2 (Figure 1a) demonstrates that it exhibits a truncated octahedral morphology, with uniform ultrathin nanosheets measuring 50~200 nm in size and displaying excellent morphological homogeneity. The high-resolution TEM (HRTEM) image of 001-TiO_2 (Figure 1b) reveals distinct lattice fringes, indicative of well-developed crystalline facets. The measured interplanar spacing of 0.352 nm corresponds to the (101) plane of anatase TiO_2, further confirming the exposure of highly active (001) crystal facets. In contrast, the TEM image of Ce/001-TiO_2 (Figure 1c) shows that after Ce doping, the material retains a more uniform and regular truncated bipyramidal octahedral morphology compared to pure TiO_2. The HRTEM image of Ce/001-TiO_2 (Figure 1d) reveals that the CeO_2 nanocrystals appear as ellipsoidal particles with diameters predominantly below 20 nm, exhibiting good dispersion. Notably, the edges of the nanosheets in Ce/001-TiO_2 appear darker than those of pure 001-TiO_2. These characterizations confirm that the individual TiO_2 units in Ce/001-TiO_2 maintain excellent crystallinity, and Ce doping does not alter the morphological characteristics or preferential exposure of the (001) crystal facets of 001-TiO_2.Energy-dispersive spectroscopy (EDS) analysis of the surface elements in Ce/001-TiO_2 (Figure 1e) demonstrates the uniform distribution of Ce, Ti, and O elements throughout the

material, with no detectable impurities. This confirms the successful incorporation of Ce, Ti, and O elements.

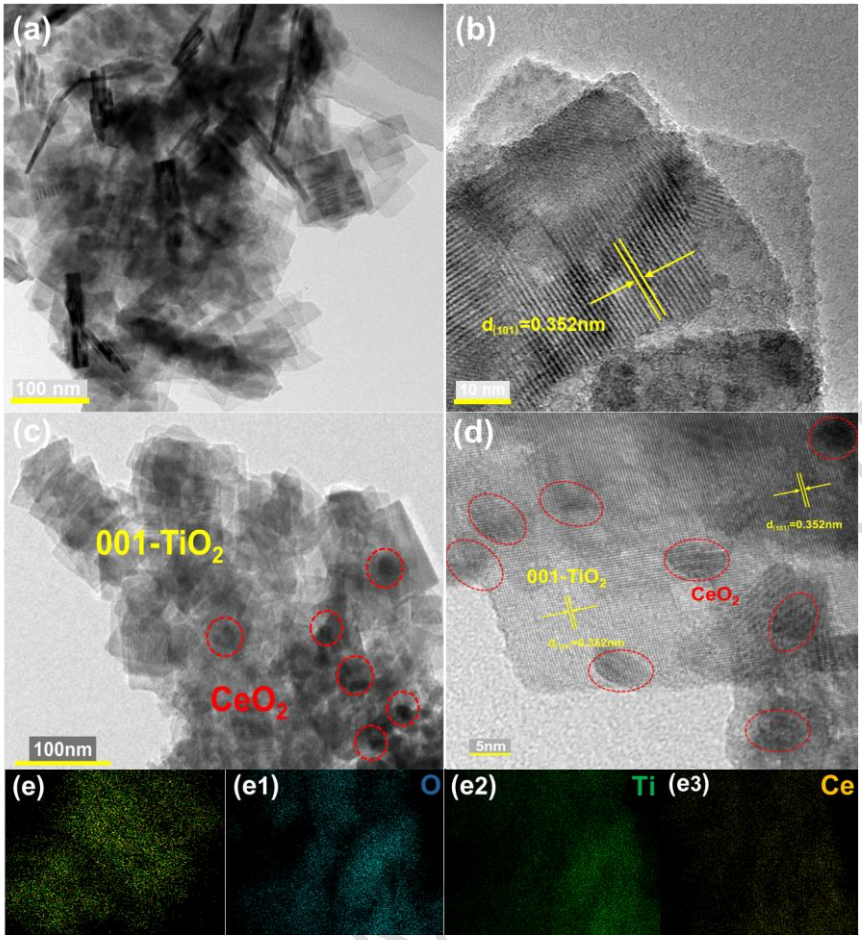

Figure 1. TEM images (a) and HRTEM images (b) of 001-TiO_2; TEM images (c) and HRTEM images (d) of Ce/001-TiO_2; EDS-mapping image (e) of Ce/001-TiO_2.

The crystal structure of the as-prepared photocatalysts was characterized by X-ray diffraction (XRD) (Figure 2a). The characteristic diffraction peaks of 001-TiO_2 at 2θ values of 25.3°, 37.5°, and 48.2° strictly correspond to the (101), (004), and (200) crystal planes of anatase TiO_2, respectively, which are in good agreement with PDF#78-2486. All samples exhibit sharp characteristic diffraction peaks, indicating high crystallinity [18]. Both Ce/001-TiO_2 and 001-TiO_2 display sharp characteristic emission peaks at (101), (005), (200), and (105) in their diffraction patterns. Notably, no characteristic peaks associated with the dopant element Ce are observed in the XRD pattern of Ce/001-TiO_2, likely due to the relatively low Ce doping content. Another plausible scenario is that Ce ions substitute for Ti or O atoms in the TiO_2 lattice or occupy interstitial sites. Given the relatively large ionic radius of Ce ions and the absence of a significant peak shift to lower angles in the XRD pattern, it is inferred—based on extensive literature reports—that Ce atoms do not incorporate into the TiO_2 lattice but are instead distributed as CeO_2 clusters on the surface and interstitial regions of TiO_2. Figure 2b presents the XPS spectrum of the Ti 2p orbital for Ce/001-TiO_2, which exhibits two distinct binding energy peaks at 458.60 eV (Ti $2p_{3/2}$) and 464.30 eV (Ti $2p_{1/2}$), indicating that Ti exists predominantly as Ti^{4+} in Ce/001-TiO_2 [19]. Figure 2c shows the XPS spectrum of the Ce 3d orbital for Ce/001-TiO_2, displaying a relatively complex pattern associated with the occupation of Ce 4f orbitals and hybridization between Ce 4f and O 2p orbitals, confirming the successful doping of Ce atoms into 001-TiO_2. Furthermore, valence band XPS (VB-XPS) analysis (Figure 2d) was conducted by extrapolating the tangent of the spectral curve to the x-axis, yielding a coordinate value of 2.12 V. This indicates that the valence band maximum (VBM) potential (E_{VBM}) of the Ce/001-TiO_2 monomer is 2.12 eV.

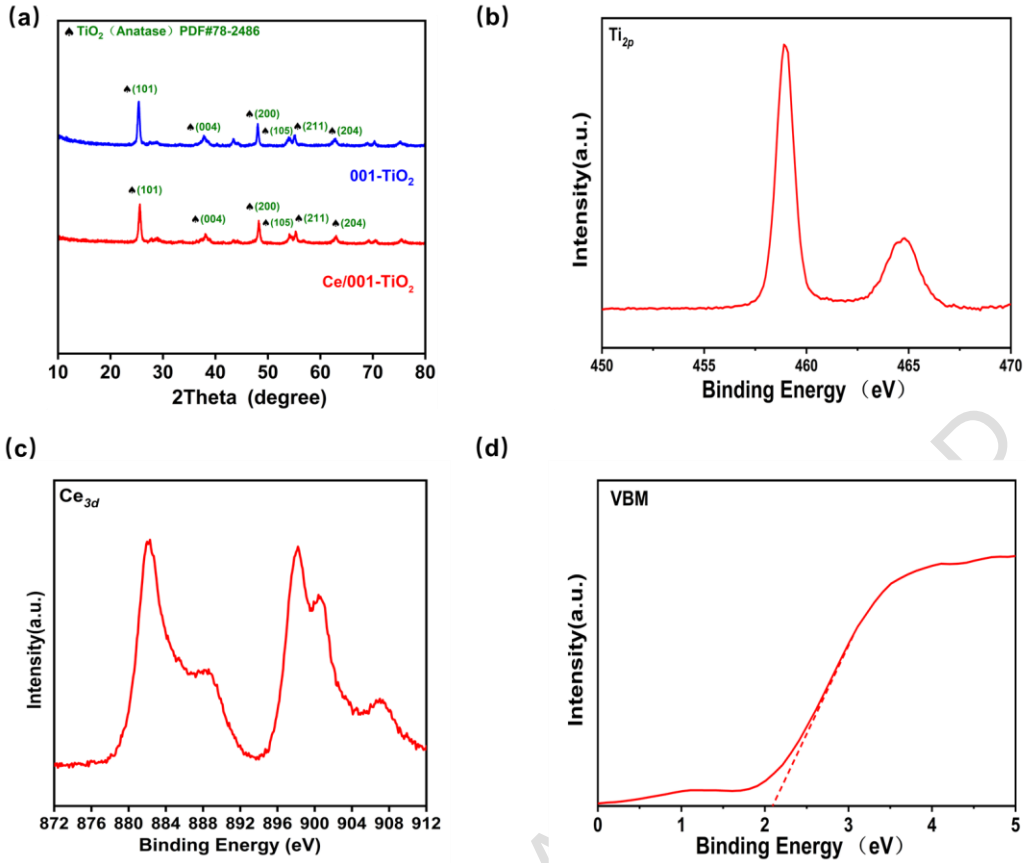

Figure 2. (a) XRD patterns of 001-TiO_2 and Ce/001-TiO_2 samples, (b) high-resolution Ti 2p XPS spectrum of the Ce/001-TiO_2 sample, (c) high-resolution Ce 3d XPS spectrum of the Ce/001-TiO_2 sample, and (d) valence band maximum (VBM) of the Ce/001-TiO_2 sample.

To thoroughly investigate the synergistic mechanism by which facet regulation of TiO_2 and Ce atom doping modification enhance photocatalytic efficiency, this study conducted a comprehensive analysis of samples including P25, 001-TiO_2, and Ce/001-TiO_2 from three aspects: fluorescence spectroscopy, photoelectrochemical, and ultraviolet-visible (UV-Vis) spectroscopy characterizations.

Through transient photocurrent (I-t) tests (Figure 3a) and electrochemical impedance spectroscopy (EIS) tests (Figure 3b), the photogenerated carrier separation efficiency and charge transfer performance in the samples were examined. The I-t tests revealed a significant gradient difference in photocurrent density, with Ce/001-TiO_2 >> 001-TiO_2 > P25. This result indicates that facet regulation effectively promotes the separation of photogenerated carriers, while Ce atom doping further enhances the interfacial charge separation efficiency. Specifically, the average photocurrent response intensity of Ce/001-TiO_2 reached 0.0009 mA/cm², which was greater than that of 001-TiO_2 (0.0006 mA/cm²) and 2.25 times that of P25 (0.0004 mA/cm²). The EIS tests showed that the order of the Nyquist curve curvature radii was consistent with that of the photocurrent density. Ce/001-TiO_2 exhibited the lowest interfacial charge transfer resistance, allowing photogenerated electrons to rapidly migrate from the bulk phase to the interface to participate in photocatalytic reactions. Both the I-t and EIS tests demonstrated that the synergistic effect of facet regulation and Ce atom doping significantly accelerated interfacial carrier separation efficiency and strongly promoted the transfer of photogenerated carriers, providing a dual driving force for enhanced photocatalytic performance.

Steady-state photoluminescence (PL) spectroscopy tests (Figure 3c) were conducted to evaluate the recombination rate of photogenerated carriers in the samples. The PL tests revealed that the fluorescence intensity of 001-TiO_2 was significantly lower than that of P25, confirming the effective suppression of electron-hole recombination by facet regulation. After further doping with Ce atoms, the fluorescence intensity of Ce/001-TiO_2 decreased markedly, indicating that Ce atom doping significantly inhibited the recombination of photogenerated carriers. The analysis from PL demonstrated that the synergistic effect of facet regulation and Ce atom doping could significantly reduce the recombination rate of photogenerated electron-hole pairs.

To further explore the light absorption characteristics and energy band structure of the photocatalysts, ultraviolet-visible diffuse reflectance spectroscopy (UV-Vis DRS) analysis (Figure 3d) was performed on the samples. The DRS results showed that P25 and pure 001-TiO_2 exhibited significant light absorption only in the ultraviolet region. After Ce doping, the light absorption band of Ce/001-TiO_2 underwent a redshift compared to TiO_2, expanding its light response range to the visible region with some absorption observed in the 400~500 nm range. The redshift of the light absorption curve may be attributed to the transition between Ce^{4+} and Ce^{3+}, where the ground-state electrons of Ce^{3+} are excited to the Ce 4f energy level by light. The bandgap energy (Eg) of the semiconductors, calculated using the Tauc plot method, revealed that the bandgap of Ce/001-TiO_2 was 2.73 eV, significantly narrower than that of 001-TiO_2 (3.10 eV). Ce atom doping improved the photoquantum efficiency of 001-TiO_2, altered the charge transfer between electrons and the 001-TiO_2 matrix, led to the formation of oxygen defects at local energy levels, and consequently narrowed the bandgap. This narrowing facilitated the full utilization of visible light and enhanced its catalytic performance.

In summary, the strategy combining facet regulation and Ce atom doping achieved efficient separation and directional migration of photogenerated charges. This strategy effectively prolonged the lifetime of photogenerated carriers. More importantly, it enabled a high flux of charges to overcome bulk recombination and migrate rapidly to the catalyst surface for redox reactions, ultimately leading to excellent photocatalytic activity.

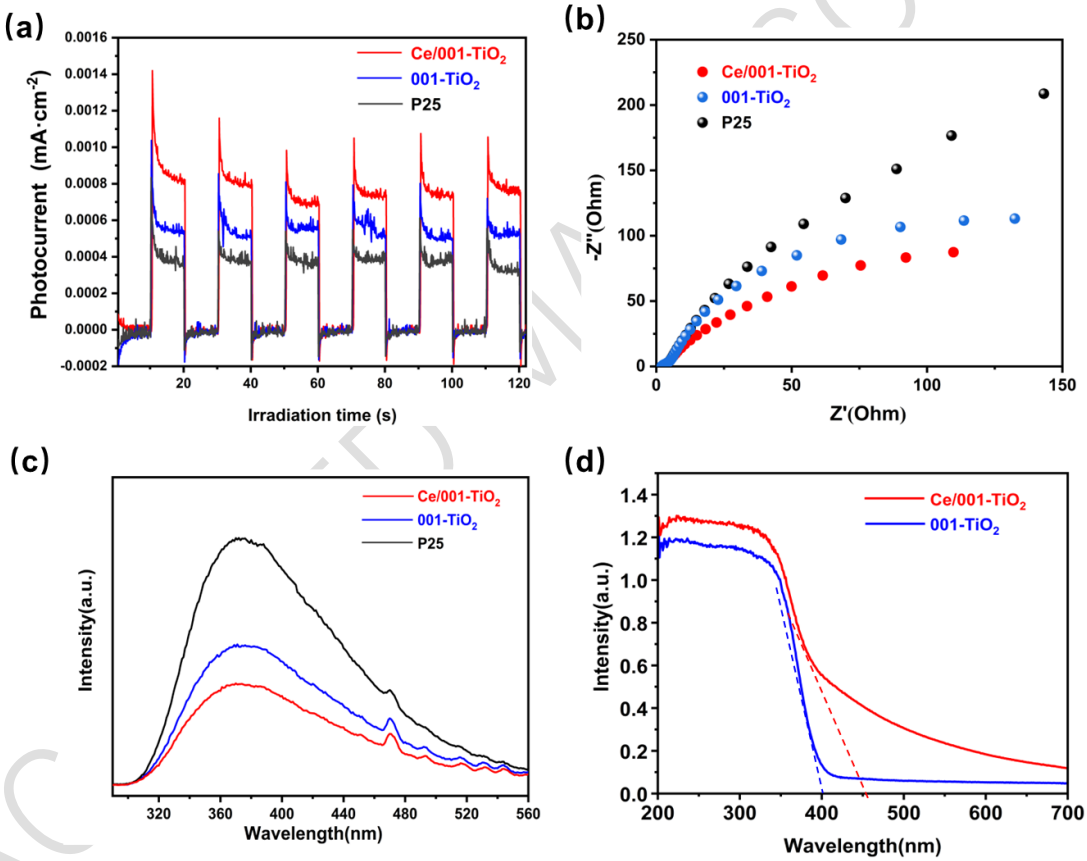

Figure 3 (a) Transient photocurrent response plots (I-t curves)，(b) Electrochemical impedance spectra，(c) Steady-state photoluminescence (PL) spectra，(d) Ultraviolet-visible diffuse reflectance spectroscopy (UV-Vis DRS)

Under simulated solar light irradiation, the photocatalytic performance of the prepared materials was evaluated (Figure 4a). In the experiments, the concentration of perfluorooctanoic acid (PFOA) in the solution was set at 5 mg/L, with a pH of 2 and a catalyst dosage of 1 g/L. The photocatalytic degradation performance of P25, 001-TiO_2, and Ce/001-TiO_2 under visible light was investigated. After 30 minutes of dark reaction, the concentration of PFOA in each sample decreased slightly due to weak adsorption on the sample surfaces. Following 240 minutes of simulated solar light irradiation, the degradation rate of P25 was only 41.7%, while that of 001-TiO_2 increased to 56.7%. This was primarily attributed to facet regulation promoting the efficient separation and transfer of photogenerated carriers. The degradation rate of Ce/001-

TiO_2 reached as high as 95.4%. This significant difference could be attributed to the synergistic effect of facet regulation and Ce atom doping, which effectively promoted the separation and migration of photogenerated carriers, enhanced the photoquantum efficiency, and thereby significantly improved the photocatalytic activity.

The pH value stands as a pivotal factor exerting influence on photocatalytic reactions. In this study, Ce/001-TiO_2 was employed as the catalyst to investigate the impact of pH on the degradation of perfluorooctanoic acid (PFOA). In a PFOA solution with an initial concentration of 4 mg/L and a constant catalyst dosage of 1 g/L, the degradation outcomes are depicted in Figure 4b. It is evident that a lower pH value within the reaction system yielded superior degradation results, aligning with the findings of this research. Specifically, under 270 minutes of light irradiation in a solution with a pH of 2, the degradation rate of PFOA soared to 95.8%. When the pH was adjusted to 3, the degradation rate dipped slightly to 84.5%. As the pH of the reaction system climbed to 4 and 5, there was a marked decline in the degradation rate. In this particular reaction system, a pH of 2 proved to be the most conducive to PFOA degradation. At this specific pH level, TiO_2 carried a greater number of positive charges, while PFOA existed in its anionic form. This charge differential facilitated the adsorption of PFOA onto the catalyst surface, enabling subsequent oxidation by active groups present on the material surface and ultimately promoting its degradation.

Light intensity also significantly affected the degradation efficiency of PFOA, as shown in Figure 4c. As the intensity of simulated visible light gradually increased, the degradation efficiency of PFOA markedly improved. This was because the increase in light intensity led to an increase in the number of photons on the photocatalyst surface per unit time, thereby enhancing the photoquantum efficiency and improving the photocatalytic efficiency. Additionally, different light sources had a significant impact on the photocatalytic degradation effect, as shown in Figure 4d. Under simulated solar light, the degradation efficiency was the highest. This was because the formation of a three-dimensional core-shell heterostructure significantly improved the utilization of visible light, while the ultraviolet light in simulated solar light could additionally excite the catalyst to generate more photogenerated charges, thereby enhancing the photocatalytic efficiency. The reusability and stability of the catalyst are important characteristics of a good catalyst. After each use of the same catalyst for photocatalytic degradation, the catalyst was centrifuged, washed, and dried for the next round of photocatalytic cycling. Stability tests (Figures 4e and 4f) showed that after five cycles of reuse, the degradation rate of the material slightly decreased but still maintained high reproducibility, with a PFOA degradation rate of 93.4%, demonstrating excellent reusability.

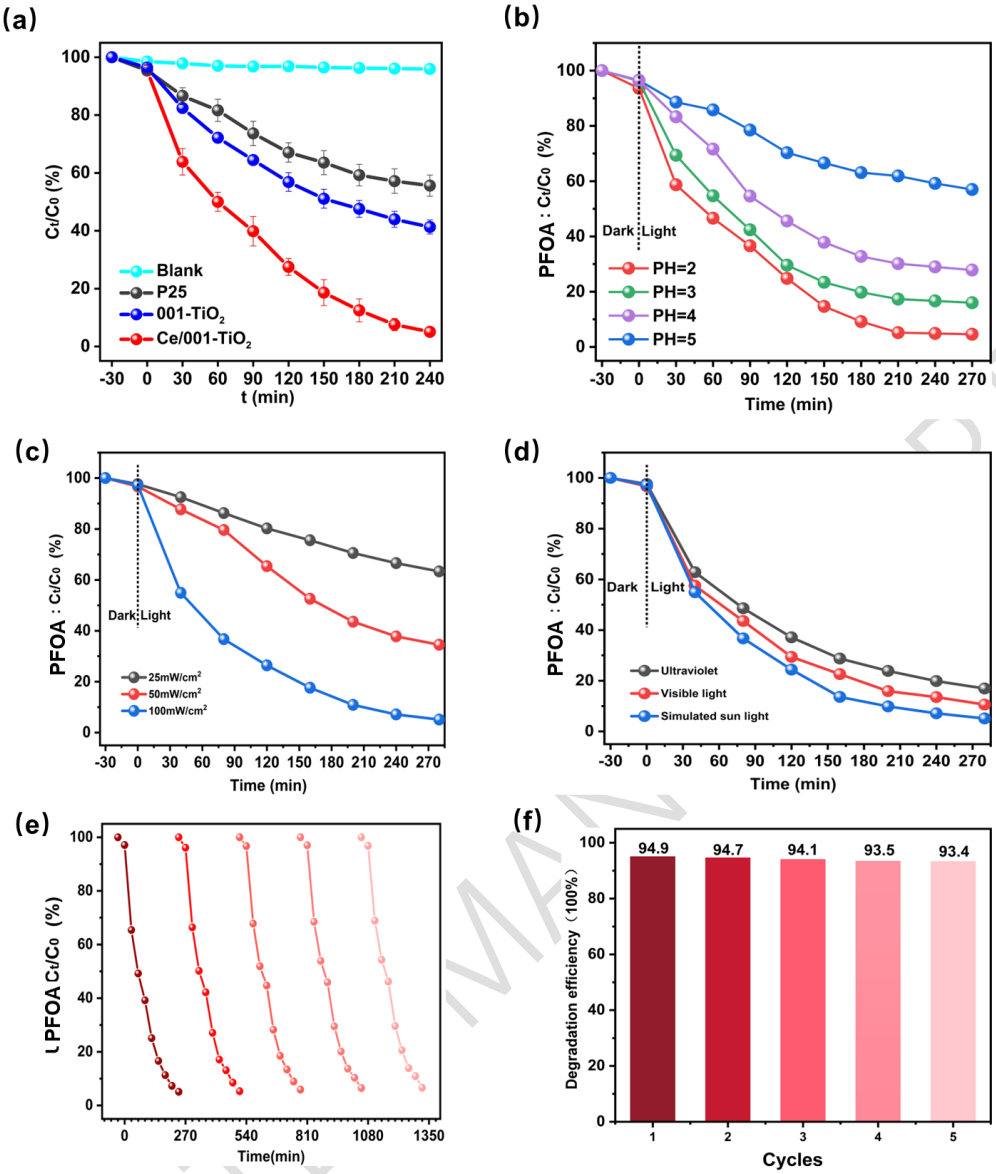

Figure 4 (a) Photocatalytic degradation curves of PFOA by P25, 001-TiO_2, and Ce/001-TiO_2, (b) Photocatalytic degradation curves of PFOA by Ce/001-TiO_2 under different pH values, (c) Photocatalytic degradation curves of PFOA by Ce/001-TiO_2 under varying light intensities, (d) Photocatalytic degradation curves of PFOA by Ce/001-TiO_2 under different light sources, (e) Photocatalytic degradation curves of PFOA by Ce/001-TiO_2 over five consecutive cycles, (f) Bar chart depicting the photocatalytic degradation of PFOA by Ce/001-TiO_2 over five cycles.

To investigate the degradation mechanism of perfluorooctanoic acid (PFOA), a PFOA wastewater degradation system incorporating only the Ce/001-TiO_2 photocatalyst was employed as a blank reference. Scavengers, including EDTA-2Na, p-benzoquinone (p-BQ), and isopropanol (IPA), were utilized to selectively neutralize the roles of photogenerated holes, $\cdot O_2^-$, and ·OH, respectively (Figures 5a and 5b). Compared to the blank reference, EDTA-2Na exhibited minimal inhibitory effect on PFOA degradation, indicating a limited contribution of photogenerated holes to PFOA degradation. Conversely, the addition of IPA and p-BQ significantly reduced the degradation efficiency to 37.7% and 48.6%, respectively, suggesting that ·OH and $\cdot O_2^-$ are the primary active species responsible for the photocatalytic degradation of PFOA, while photogenerated holes play a secondary role.

Furthermore, electron paramagnetic resonance (EPR) spectroscopy was employed to further elucidate the specific mechanism of the photocatalytic process. Under simulated solar light irradiation, Figure 5c demonstrates that both Ce/001-TiO_2 and 001-TiO_2 exhibit distinct characteristic quartet signals of DMPO-·OH. Notably, Ce/001-TiO_2 displays a stronger signal, indicating a higher production of ·OH. Figure 5d reveals that Ce/001-TiO_2 exhibits a pronounced characteristic sextet signal of DMPO-$\cdot O_2^-$ under

simulated solar light irradiation, suggesting a high yield of $\cdot O_2^-$. In contrast, 001-TiO_2 does not show a distinct characteristic sextet signal, indicating its limited ability to generate $\cdot O_2^-$.

In summary, both EPR spectroscopy and radical scavenger experiments consistently demonstrate that doping Ce atoms onto 001-TiO_2 effectively promotes the separation of photogenerated electron-hole pairs, enabling efficient conversion of photogenerated charges in the excited state into catalytically active species and facilitating the generation of oxygen vacancies. These findings confirm that the primary active species responsible for PFOA degradation are ·OH and $\cdot O_2^-$, while photogenerated holes play a minor role.

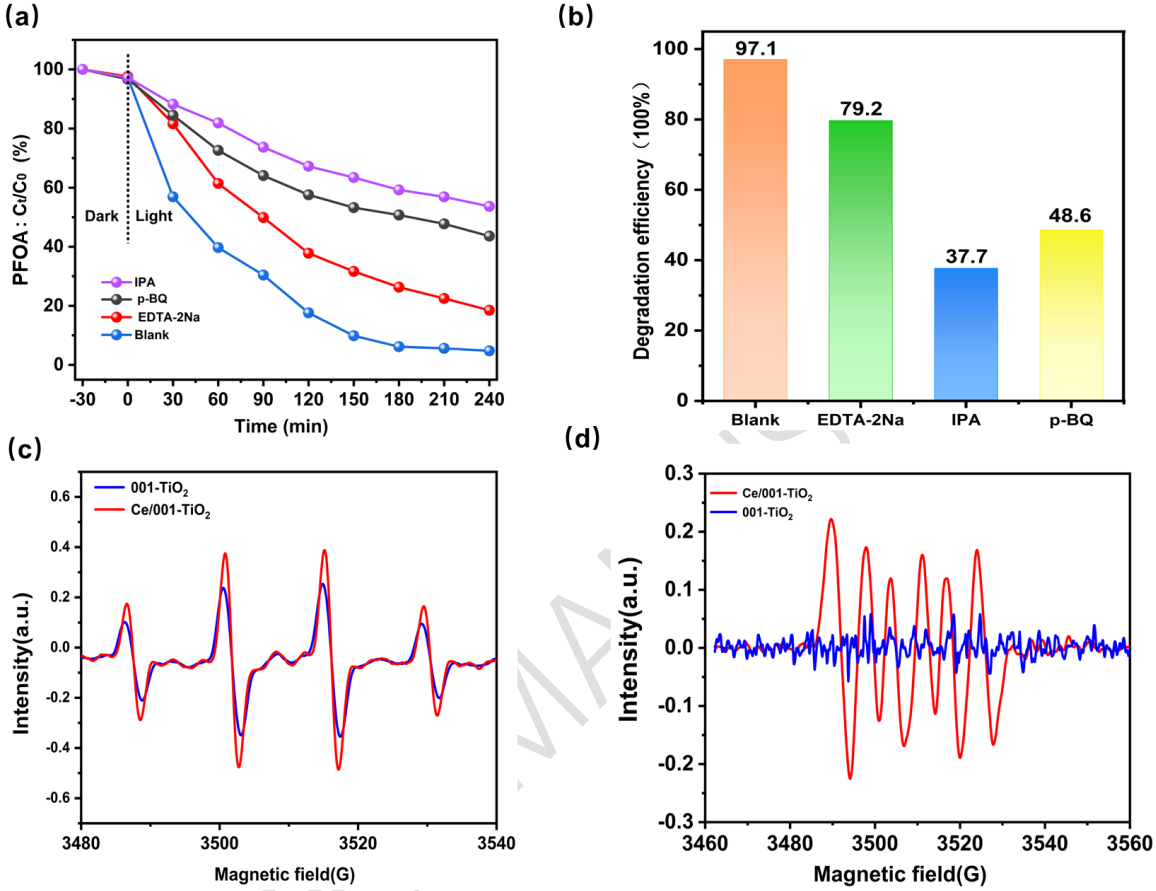

Figure 5 (a) PFOA curve for photocatalytic degradation of Ce/001-TiO_2 for 240min under conditions of capture agent available for different active species，(b) Bar chart depicting the photocatalytic degradation of PFOA by Ce/001-TiO_2 for 240min under conditions of capture agent available for different active species，(c) DMPO-·OH EPR signal, (d) DMPO-$\cdot O_2^-$ EPR signal

Based on the morphological and structural analysis of the photocatalyst, spectral absorption performance, radical trapping experiments, and EPR analysis, it has been confirmed that Ce^{3+} doping enhances the visible-light response of 001-TiO_2 and increases the yield of photogenerated electrons. The energy band edge positions of the photocatalyst can be calculated using the formula $E_{CB}=E_{VB}-E_g$. The energy band structure of the Ce/001-TiO_2 photocatalyst is illustrated in Figure 6. Combining spectral absorption performance and VB-XPS spectra, the E_{VB} of Ce/001-TiO_2 was determined to be 2.12 eV. From UV-Vis DRS, Eg was found to be 2.73 eV, leading to a calculated E_{CB} of -0.61 eV. Both the E_{CB} values before and after doping are more negative than the oxidation potential of $O_2/\cdot O_2^-$ (-0.046 eV vs. NHE), enabling the highly reductive electrons on the conduction band to directly reduce O_2 to generate $\cdot O_2^-$. Simultaneously, Ce^{3+} reacts with surface-adsorbed oxygen to produce $\cdot O_2^-$, and surface oxygen vacancies act as electron trapping sites to further promote $\cdot O_2^-$ generation. After doping, the E_{VB} is higher than that of $OH^-/\cdot OH$ (1.99 eV vs. NHE), allowing photogenerated holes to oxidize OH^- to generate ·OH. In pure 001-TiO_2, under UV excitation, an electron transition occurs from the O 2p to Ti 3d orbitals. Ce doping can improve the surface structure of 001-TiO_2 and introduce impurity energy levels within the bandgap of 001-TiO_2, reducing its bandgap width and causing a redshift in its spectral absorption range, thereby further enhancing visible-light utilization. Additionally, due to the unique 4f electron configuration of Ce, Ce^{4+} can capture electrons ($Ce^{4+}+e^-\rightarrow Ce^{3+}$), and the resulting Ce^{3+} can also combine with holes ($Ce^{3+}+h^+\rightarrow Ce^{4+}$), effectively

suppressing the recombination of photogenerated electron-hole pairs [20-22]. The abundant oxygen vacancies and redox conversion between Ce^{3+}/Ce^{4+} in Ce/001-TiO_2 effectively promote rapid photogenerated electron transfer, reducing the recombination probability of photogenerated electrons and holes. Active radical trapping experiments demonstrate that $\cdot O_2^-$ and ·OH are the primary active species in the degradation of PFOA, while the contribution of photogenerated holes is relatively low. Therefore, the proposed degradation mechanism of PFOA is as follows: PFOA exists as an anion in the reaction system, and Ce/001-TiO_2 surfaces carry a large amount of positive charge under acidic conditions, facilitating the adsorption of PFOA onto the material surface. Under the combined action of active species such as $\cdot O_2^-$ and ·OH, a continuous photocatalytic degradation system is formed, enabling PFOA and its byproducts to undergo stepwise transformation and ultimately be mineralized into CO_2, H_2O, and other non-toxic small molecules.

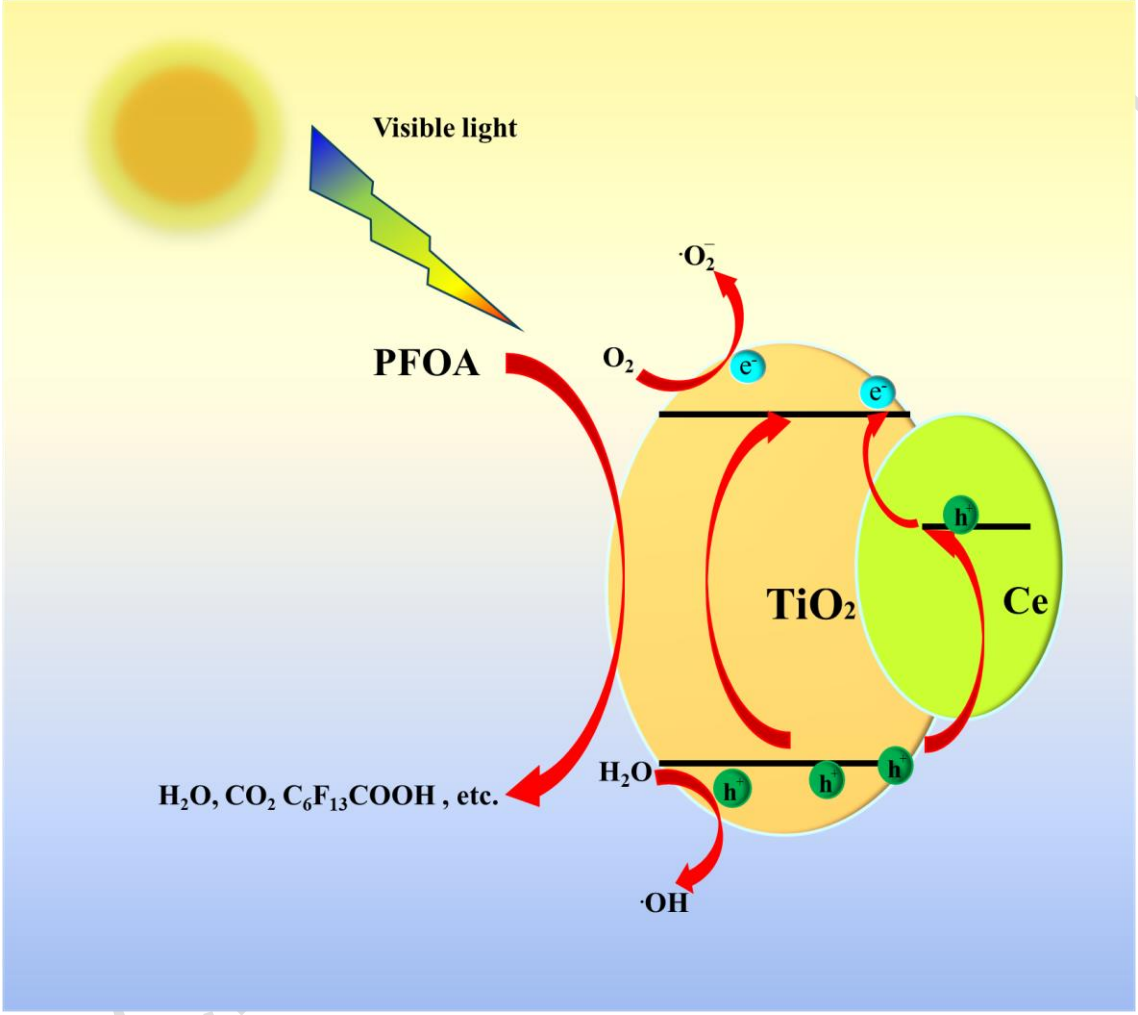

Figure 6 Schematic Illustration of Photocatalytic Degradation of PFOA

4 Conclusions

In summary, this study successfully synthesized Ce/001-TiO_2 via a solvothermal method. Metal doping combined with interface engineering synergistically narrowed the bandgap, leading to a redshift and enhancement in light absorption. This modification concurrently suppressed electron-hole recombination, markedly improving the charge separation efficiency. When employed for the degradation of simulated PFOA wastewater under visible light irradiation, Ce/001-TiO_2 demonstrated superior performance compared to single 001-TiO_2 and P25. Under optimal experimental conditions, Ce/001-TiO_2 achieved a 95.4% degradation efficiency for high-concentration PFOA wastewater (5 mg/L) within 240 minutes. Furthermore, after five consecutive reuse cycles, the degradation rate of PFOA remained as high as 93.4%, confirming the stable and efficient photocatalytic performance of this composite material. Notably, ·OH and $\cdot O_2^-$ were identified as the primary active species in the photocatalytic reaction system. This work not only delivers a novel and practical approach for efficient PFOA removal from wastewater but also paves the way for the rational design of high-performance photocatalysts. Future efforts may explore the application of such high-efficiency catalysts in the treatment of other emerging contaminants, such as perfluorooctanesulfonate

(PFOS) and antibiotics, thereby contributing to water pollution control and the achievement of carbon neutrality goals.

Funding: Not applicable.
Data availability statement: All the associated data are including within the manuscript, further request can directly to the corresponding author.
Conflict of interest: Authors declare there are no conflict of interest.

References

[1] Norsham I N M, Sambasevam K P, Shahabuddin S, et al. Photocatalytic degradation of perfluorooctanoic acid (PFOA) via MoS_2/rGO for water purification using indoor fluorescent irradiation[J]. Journal of Environmental Chemical Engineering, 2022, 10(5): 108466.
[2] Ilić N, Andalib A, Lippert T, et al. Ultrasonic degradation of GenX (HFPO-DA)–Performance comparison to PFOA and PFOS at high frequencies[J]. Chemical Engineering Journal, 2023, 472: 144630.
[3] Jaafar A D, Graish M S, Alatabe M J A, et al. Sustainable water production study from simulation humid air by condensation unit[J]. Desalination and Water Treatment, 2024, 320: 100885.
[4] Wen Y, Rentería-Gómez Á, Day G S, et al. Integrated photocatalytic reduction and oxidation of perfluorooctanoic acid by metal–organic frameworks: key insights into the degradation mechanisms[J]. Journal of the American Chemical Society, 2022, 144(26): 11840-11850.
[5] Yao M ,Shen J ,Yang H , et al.Microwave heating:A new high efficiency and low energy-consumption option for removing PFOA and PFOS from soil.[J].Journal of environmental management,2025,391126402.
[6] Biswas S, Wong B M. Degradation of perfluorooctanoic acid on aluminum oxide surfaces: new mechanisms from ab initio molecular dynamics simulations[J]. Environmental Science & Technology, 2023, 57(16): 6695-6702.
[7] Kang H K ,Son C ,Bae S , et al.Investigation of perfluorooctanoic acid and perfluorooctane sulfonate adsorption by Ca- and Fe-modified biochars: Potential of Ca-modified biochar in real water matrices[J].Separation and Purification Technology,2025,376(P1):133906-133906.
[8] Zhang P ,Bai R ,Guo Y , et al.Innovative modification of bacterial cellulose membrane for high-efficient removal of PFOA substances from water[J].Separation and Purification Technology,2025,376(P2):133967-133967.
[9] YiZhi Z ,Feng Z ,Yuan G .Bi_2O_3 modified TiO_2 nanotube arrays and their application towards unsymmetrical dimethylhydrazine degradation in wastewater by electroassisted photocatalysis.[J].RSC advances,2023,13(5):2993-3003.
[10] Ren X ,Zeng Y .A study on interfacial regulation and function mechanism of TiO_2@CeO_2 3D core-shell heterostructure for photocatalytic degradation of unsymmetrical dimethyl hydrazine[J].Applied Surface Science,2024,677160781-160781.
[11] Zeng Y Z, Ren X H. Preparation of mesoporous TiO_2 nanomaterials doped with rare earth ions (La^{3+}, Sm^{3+}, Nd^{3+}, Gd^{3+}) and its application in the photodegradation of unsymmetrical dimethylhydrazine wastewater[J]. Global Nest Journal, 2023, 25(10): 81-92.
[12] Ralf D ,Detlef B ,Hisao H .Light-induced degradation of perfluorocarboxylic acids in the presence of titanium dioxide.[J].Chemosphere,2007,67(4):785-92.
[13] Nguyen C K, Cha H G, Kang Y S. Axis-oriented, anatase TiO_2 single crystals with dominant {001} and {100} facets[J]. Crystal growth & design, 2011, 11(9): 3947-3953.
[14] Dan-Ni P ,Li G ,Ai-Yong Z , et al.Defective titanium dioxide single crystals exposed by high-energy {001} facets for efficient oxygen reduction.[J].Nature communications,2015,6(Oct.):8696.
[15] Dong H ,Zeng G ,Tang L , et al.An overview on limitations of TiO_2-based particles for photocatalytic degradation of organic pollutants and the corresponding countermeasures[J].Water Research,2015,79128-146.
[16] Al-Shawafi W M, Salah N, Alshahrie A, et al. Size controlled ultrafine CeO_2 nanoparticles produced by the microwave assisted route and their antimicrobial activity[J]. Journal of Materials Science: Materials in Medicine, 2017, 28(11): 177.
[17] Xin T ,Chaohe Z ,Haibo Z .Ce-modified $SrFeO_3$-δ for ethane oxidative dehydrogenation coupled with CO_2 splitting via a chemical looping scheme[J].Applied Catalysis B: Environmental,2022,303
[18] Tianyan Z ,Huangxin L ,Tianming Z , et al.Self-powered/self-cleaned atmosphere monitoring system from combining hydrovoltaic, gas sensing and photocatalytic effects of TiO_2 nanoparticles[J].Journal of Materials Science & Technology,2021,7633-40.

[19] Jianglong M ,Danyang L ,Hui M , et al.Synergistic wide spectrum response and directional carrier transportation characteristics of Se/$SnSe_2$/TiO_2 multiple heterojunction for efficient photoelectrochemical simultaneous degradation of Cr (VI) and RhB[J].Applied Surface Science,2021,542148673-.
[20] Zeng Y, Ren X. A study on interfacial regulation and function mechanism of S-scheme 001-TiO_2/CeO_2 two-dimensional charge-separation Interface for photocatalytic degradation of unsymmetrical Dimethylhydrazine[J]. Journal of Photochemistry and Photobiology A: Chemistry, 2025: 116818.
[21] Zeng Y, Ren X. Highly efficient photocatalytic degradation of unsymmetrical dimethylhydrazine with 001-TiO_2/CeO_2 S-scheme heterojunction[J]. Applied Surface Science, 2025: 164499.
[22] Alatabe M J A, Jaafar A D, Kariem N O, et al. Effective adsorption of Chromium (III) ions from the tannery effluent wastewater using Cerium Oxide (CeO2) nanoparticles[J]. Indian Chemical Engineer, 2025: 1-18.